INTERNATIONAL JOURNAL FOR NUMERICAL METHODS IN FLUIDS
Int. J. Numer. Meth. Fluids 2006; **50**:219–234
Published online 1 September 2005 in Wiley InterScience (www.interscience.wiley.com). DOI: 10.1002/fld.1051

Meshless numerical simulation for fully nonlinear water waves

Nan-Jing Wu[§,¶], Ting-Kuei Tsay[*,†,‡] and D. L. Young[‡,‖]

Department of Civil Engineering, National Taiwan University, Taipei 106, Taiwan

SUMMARY

A meshless numerical model for nonlinear free surface water wave is presented in this paper. An approach of handling the moving free surface boundary is proposed. Using the fundamental solution of the Laplace equation as the radial basis functions and locating the source points outside the computational domain, the problem is solved by collocation of only a few boundary points. Present model is first applied to simulate the generation of periodic finite-amplitude waves with high wave-steepness and then is employed to simulate the modulation of monochromatic waves passing over a submerged obstacle. Good agreements are observed as compared with experimental data and other numerical models. Copyright © 2005 John Wiley & Sons, Ltd.

KEY WORDS: meshless numerical method; nonlinear water waves; moving boundary; radial basis functions; method of fundamental solutions

1. INTRODUCTION

In the past decades, extensive works have been carried out to simulate the propagation problems of surface gravity water waves. Among these works, perturbation techniques are usually employed to simplify the moving and fully nonlinear free surface boundary conditions. After perturbation work is undertaken, the difficulty of free surface boundary condition is circumvented by a fixed boundary which becomes weakly nonlinear in time domain [1–3] as well as in frequency domain [4–7]. Perturbation approaches, always accompanying with complicated, prolix and tedious equations and scheme formulations, might lose some degrees of accuracy and fail to treat the fully nonlinear wave problems well. Without simplification through perturbation procedure, solving the water wave problems directly will encounter the situation

*Correspondence to: Ting-Kuei Tsay, Department of Civil Engineering, National Taiwan University, 1, Sec. 4, Roosevelt Rd., Taipei 106, Taiwan.
†E-mail: tktsay@sun.epa.gov.tw
‡Professor.
§E-mail: d90521005@ntu.edu.tw
¶PhD candidate.
‖E-mail: dlyoung@hy.ntu.edu.tw

Received 12 November 2004
Revised 26 April 2005
Accepted 3 May 2005

that the boundary at the moving free surface is fully nonlinear and not known *a priori*. For traditional numerical methods (such as FEM or FDM for example), non-fixed (deforming) meshes are needed [8, 9]. Usually, an excess number of nodes and a huge size of matrix accompany with the formulation if one tries to solve the problem by conventional numerical methods. Time-domain boundary element method (BEM) had been employed for its applicability to the computation of steep water wave propagation since nonlinear free surface conditions were fully incorporated [10–16]. By the mixed Eulerian–Lagrangian (MEL) approach, particle trajectories and the nonlinear boundary conditions on the free surface can be predicted after numerical integration in the time domain, then the velocity potential of linear boundary value problem can be solved directly at the further time step. The MEL approach was explicated in detail in the paper of Tsai and Yue [17]. Overturning waves can even be simulated by means of MEL approach [10, 16]. As BEM is based on solving integral equations, integration along the boundaries are always needed. Evaluating these integrals is a tedious task since there are singularities on the boundaries, either fixed or moving. Furthermore, BEM produces huge and dense matrices, which take much time in solving the linear algebraic system. Though the dense matrices can be efficiently compressed to sparse ones by some means of approximation such as fast multipole method, panel clustering and wavelet compression [18–20], to speed up the computations, the need of computing tedious singular integrals still remains in BEM with some difficulties for implementing free surface water wave problems.

In recent years, a new numerical technique called 'meshless methods' (or 'mesh-free methods', or 'mesh reduction methods') has been exploited under strong developments. This scheme has attracted great attention from science and technology communities. A common feature of meshless methods is that neither domain nor surface meshing is required during the solution process in solving boundary and initial value problems. Thus, they are suitable to handle physical problems with large deformation, moving boundaries, and a complicated geometry of the solution domain.

The basic idea of meshless method is the construction of radial basis functions (RBF) which state the relationship between the two-point distances. The RBFs were first developed for interpolating scattered data [21, 22], and later became a kind of artificial neural network kernels [23]. The applications of the concepts of RBFs to solve PDEs have been introduced for years [24]. This approach was also recently applied to modelling the shallow water equations in the coastal engineering [25]. Generally speaking, there are two kinds of meshless methods: the domain-type and the boundary-type methods. In the domain meshless method, such as the Kansa's method, any single RBF does not satisfy the governing equations, and there must be a large number of collocation points in both the computational domain as well as boundary to obtain a better solution. Thus, neither the number of nodes nor the size of matrix is reduced too much, and the advantages of domain meshless approach are just for easy programming and avoiding the chore of mesh generation. On the other hand, in the boundary meshless method in some PDEs (such as Laplace, Helmholtz, etc. for example), one can choose the fundamental solution of the linear operator to be the RBF [26], which will automatically satisfy the governing equation except at the centre of RBF. If all the source points (centres of RBF) are set outside the computational domain, there will be no singularity in the computational domain at all and only a few collocation points on the boundary are needed to solve the problems by the method of collocation. In other words, by using the method called the method of fundamental solutions (MFS), the governing equation has been satisfied automatically and the remaining task is only to satisfy the boundary conditions. This

method is also called MFS. As a consequence, the solution procedures are only limited to collocating the boundary conditions and become very simple and also very easy to program as well. Though MFS is based on the fundamental solution as well as BEM, non-needing of numerical integration makes it more effective in both manpower and computer-operation reduction.

The intention of this study is thus to use the MFS to deal with the simulations of two-dimensional fully nonlinear water wave problems and to compare with experimental works and other numerical models.

2. GOVERNING EQUATION AND BOUNDARY CONDITIONS

The problem of a free surface water wave propagating in a flume can be considered as a 2-D hydrodynamic problem for the inviscid, irrotational and incompressible fluids with free surface boundary. Thus, there exists a velocity potential satisfying the Laplace equation

$$\frac{\partial^2 \phi}{\partial x^2} + \frac{\partial^2 \phi}{\partial z^2} = 0 \tag{1}$$

where $\phi(x,z,t)$ is the velocity potential.

At the free surface, the boundary conditions are specified by

$$\left.\frac{\partial \phi}{\partial z}\right|_{z=\eta} = \frac{\partial \eta}{\partial t} + \left.\frac{\partial \phi}{\partial x}\right|_{z=\eta} \frac{\partial \eta}{\partial x} \tag{2}$$

$$\left.\frac{\partial \phi}{\partial t}\right|_{z=\eta} = -g\eta - \frac{1}{2}\left.\left(\left(\frac{\partial \phi}{\partial x}\right)^2 + \left(\frac{\partial \phi}{\partial z}\right)^2\right)\right|_{z=\eta} \tag{3}$$

where $\eta(x,t)$ is the free surface displacement. The above two equations are called the kinematic and dynamic free surface boundary conditions (K.F.S.B.C and D.F.S.B.C), respectively.

At the bottom, the boundary condition is the no-flux condition. That is,

$$\left.\frac{\partial \phi}{\partial z}\right|_{z=-h} = -\left.\frac{\partial \phi}{\partial x}\right|_{z=-h} \frac{\mathrm{d}h}{\mathrm{d}x} \tag{4}$$

where $h(x)$ is the water depth.

The boundary condition at the wave generator is

$$\left.\frac{\partial \phi}{\partial x}\right|_{x=\xi} = \frac{\mathrm{d}\xi}{\mathrm{d}t} \tag{5}$$

where $\xi(z,t)$ is the position of the wave paddle.

The boundary condition at the end of the flume is treated as the radiation boundary condition, which means waves are always outgoing. It is shown as

$$\left.\frac{\partial \phi}{\partial x}\right|_{x=x_r} = -\left.\left(\frac{1}{C}\frac{\partial \phi}{\partial t}\right)\right|_{x=x_r} \tag{6}$$

where C is the wave speed.

Now that we have governing equation and boundary conditions, the problem is well posed and can be solved numerically.

3. NUMERICAL IMPLEMENTATION

The numerical solution at each time step is assumed as the linear combination of N RBFs, taking nth time step as example

$$\phi^{(n)}(x,z) = \sum_{i=1}^{N} \alpha_i^{(n)} q_i(x,z) \tag{7}$$

where $q_i(x,z)$ is the RBF whose centre (also named source point) is at (x_i, z_i), and $\alpha_i^{(n)}$ is its weight. The type of RBF chosen in this study is the fundamental solution of a 2-D Laplace operator. That is,

$$q_i(x,z) = \ln(r_i) \tag{8}$$

where $r_i = \sqrt{(x-x_i)^2 + (z-z_i)^2}$ is the distance from any position in the computational domain to that specific RBF centre. Thus, the solution form satisfies the governing equation automatically except at the RBF centres. If all the RBF centres are chosen out of the computational domain, the solution can be obtained by solving $\alpha_i^{(n)}$ from the matrix collocated from the boundary conditions only.

The free surface boundary conditions involving the time variable (Equations (2) and (3)) can be formulated by the second order finite difference formulations

$$\eta^{(n+1)} = \eta^{(n-1)} + 2\Delta t \left(\left.\frac{\partial \phi}{\partial z}\right|_{z=\eta} - \left.\frac{\partial \phi}{\partial x}\right|_{z=\eta} \frac{\partial \eta}{\partial x} \right)^{(n)} \tag{9}$$

$$(\phi|_{z=\eta})^{(n+1)} = (\phi|_{z=\eta})^{(n-1)} - 2\Delta t \left(g\eta + \frac{1}{2} \left(\left(\frac{\partial \phi}{\partial x}\right)^2 + \left(\frac{\partial \phi}{\partial z}\right)^2 \right) \Bigg|_{z=\eta} \right)^{(n)} \tag{10}$$

The boundary condition at the free surface can be applied directly when solving ϕ for the $(n+1)$th time step. This approach is rather straightforward, without any iteration. Unlike the MEL approach, this approach is more effective since no time-domain integrations are needed. However, as we treat the free surface displacement as a function of the horizontal plane, the overturning waves could not be simulated.

Based on the solution form in Equation (7), the partial derivatives of the velocity potential are shown as

$$\left(\frac{\partial \phi}{\partial x}\right)^{(n)} = \sum_{i=1}^{N} \alpha_i^{(n)} \frac{\partial q_i}{\partial x} \tag{11}$$

$$\left(\frac{\partial \phi}{\partial z}\right)^{(n)} = \sum_{i=1}^{N} \alpha_i^{(n)} \frac{\partial q_i}{\partial z} \tag{12}$$

The boundary conditions at the wave paddle and bottom are then applied properly. Furthermore, the boundary condition at the end of the flume can also be applied as

$$\phi^{(n+1)} + \frac{C\Delta t}{2}\left(\frac{\partial\phi}{\partial x}\right)^{(n+1)} = \phi^{(n)} - \frac{C\Delta t}{2}\left(\frac{\partial\phi}{\partial x}\right)^{(n)} \tag{13}$$

At each time step, there are N unknowns $(\alpha_i^{(n)}, i = 1,\ldots,N)$ to be solved. Thus, N boundary points are needed for the method of collocation. Boundary points at the free surface are coded from 1 to N_s, which is the count of surface boundary points. The gradient of free surface displacement at any specific boundary point can be approximated by a second order finite difference scheme as

$$\left(\frac{\partial\eta}{\partial x}\right)_j^{(n)} = \begin{cases} \dfrac{-\eta_{j+2}^{(n)} + 4\eta_{j+1}^{(n)} - 3\eta_j^{(n)}}{2\Delta x}, & j = 1 \\ \dfrac{\eta_{j+1}^{(n)} - \eta_{j-1}^{(n)}}{2\Delta x}, & j = 2,\ldots,N_s - 1 \\ \dfrac{\eta_{j-2}^{(n)} - 4\eta_{j-1}^{(n)} + 3\eta_j^{(n)}}{2\Delta x}, & j = N_s \end{cases} \tag{14}$$

The procedure of numerical implementation is shown in Figure 1 and is illustrated as follows:

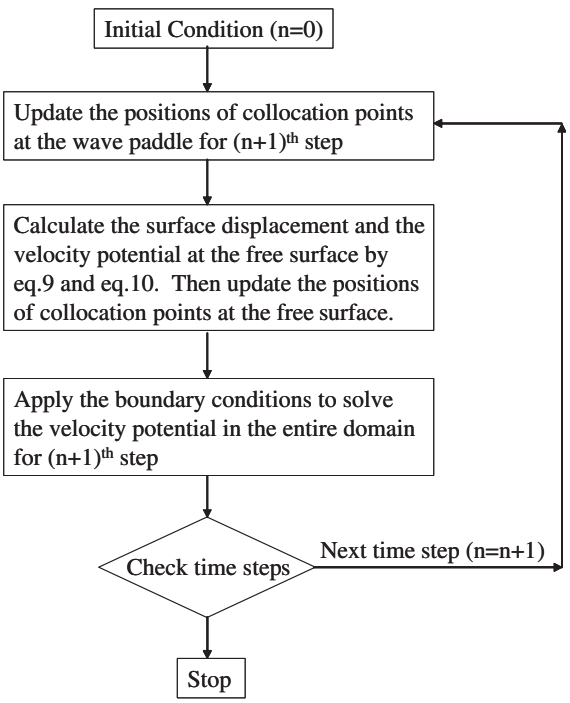

Figure 1. The flow chart of numerical simulation.

Step 1: The velocity potential in the entire domain ϕ and the particle displacement at the free surface η are all set to zero, initially (at $n=-1$ and $n=0$).

Step 2: The positions of collocation points at the wave paddle for $(n+1)$th time step are updated.

Step 3: The free surface displacement and velocity potential at the free surface are calculated by Equations (9) and (10). Then, the positions of collocation points at the free surface for $(n+1)$th time step are updated.

Step 4: Calculating the partial derivatives of the RBFs at all collocation points, the boundary conditions at the free surface, the bottom and two ends of the flume are then applied. And the solution of the velocity potential in the entire domain at $(n+1)$th time step can thus be obtained.

Step 5: The number of time steps proceeded is checked. If the requirement of time steps is not achieved, step 2 for the next time step is then processed.

4. MODEL APPLICATIONS

Present numerical model is applied to two types of wave motion problems. First, the finite-amplitude, high steep waves generated by a harmonically oscillating paddle of piston-type wavemaker are simulated. The numerical solutions of periodic wave generation are compared with those of linear (or small amplitude) wave theory and experimental data [27]. Then the modulation of monochromatic waves passing over a submerged obstacle is simulated. The numerical results of monochromatic waves passing over a submerged obstacle are compared with experimental data [28] and two other numerical results [29, 30].

4.1. Periodic wave generation

The waves generated by a finite-amplitude harmonically oscillating paddle of piston-type wavemaker were observed and discussed by Ursell *et al.* [27]. The wave heights were less than predicted by small-amplitude wave theory because of the finite-amplitude effects. Ursell *et al.* [27] carried out 20 runs for small-amplitude waves, and 4 runs for high steep waves. The experimental works were to test the validation of small-amplitude wave theory and also to find the finite-amplitude effects on the wave characteristics. The wave conditions included the wave period T, water depth h, wave height, H, and the wavemaker stroke S for high wave-steepness, as listed in Table I. The length of our numerical wave flume is 20 m. The paddle position of the piston-type wavemaker in numerical model is a function of time as

$$\xi(t)=\frac{S}{2}\sin\omega t \tag{15}$$

Table I. List of Ursell *et al.*'s [27] finite-amplitude wave generation conditions.

Run	T (s)	S (cm)	h (ft)	H_{measured} (cm)
21	0.79	2.54	2.00	4.77
22	0.85	3.15	1.50	5.25
23	0.95	4.50	1.00	5.47
24	0.96	5.73	0.66	5.14

The arrangement of source points and boundary points is shown in Figure 2. Horizontal spacing of adjacent boundary points along the free surface is 0.1 m (about 1/10–1/13 wave length). There are 406 source points outside the computational domain. The interval of numerical time step is in the order of 1/50 wave period. When simulation time achieves several wave periods, quasi-steady solution near the wave paddle can be obtained (Figure 3), and then the wave height at each specific position can be calculated by subtraction of the lowest water level from the highest during the time interval of one wave period. In present work, the wave heights are calculated from the free surface displacement during $t = 20T$–$21T$. The wave height distributions near the wave paddle are shown in Figure 4. One can find that the evanescent waves are significant near the wave paddle for short wave cases. Since the actual position of wave gage was not mentioned by Ursell *et al.* [27], we calculate the average

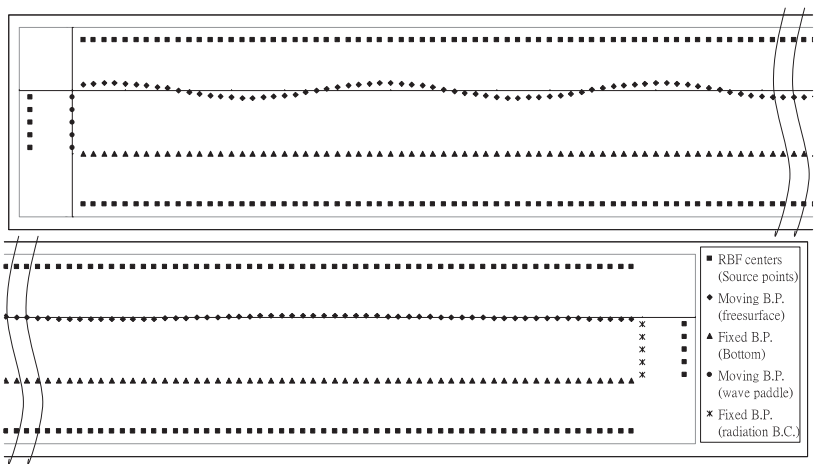

Figure 2. The arrangement of source and boundary points.

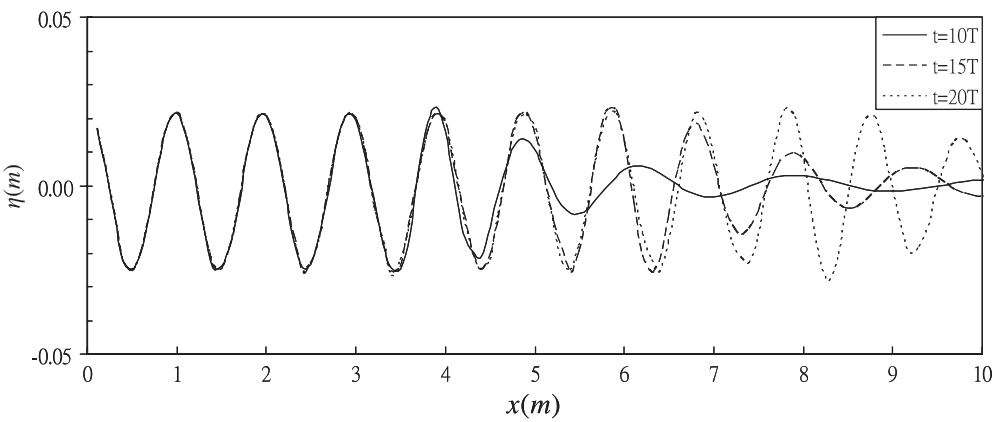

Figure 3. Free surface displacement nearby the wave paddle at $t = 10\,T$, $t = 15\,T$ and $t = 20\,T$ for the case of $T = 0.79$ s, $S = 2.54$ cm, $h = 2.00$ ft.

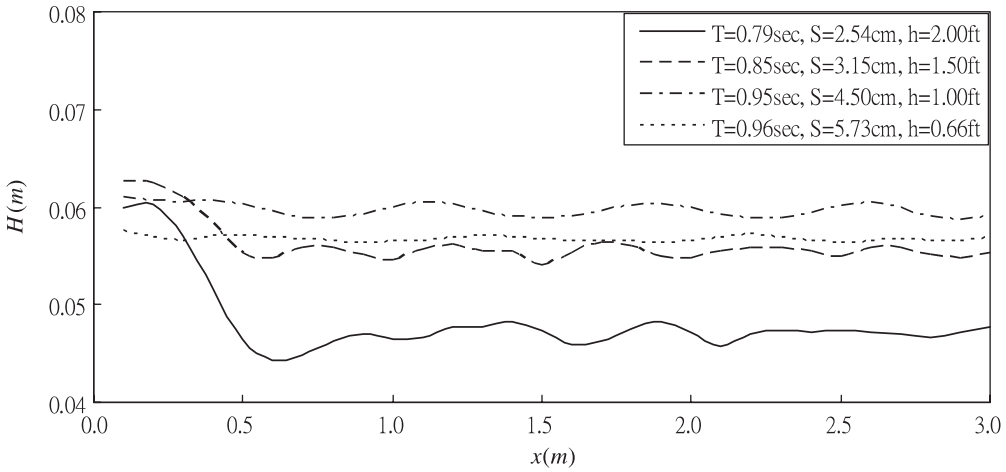

Figure 4. Wave height distributions near the wave paddle.

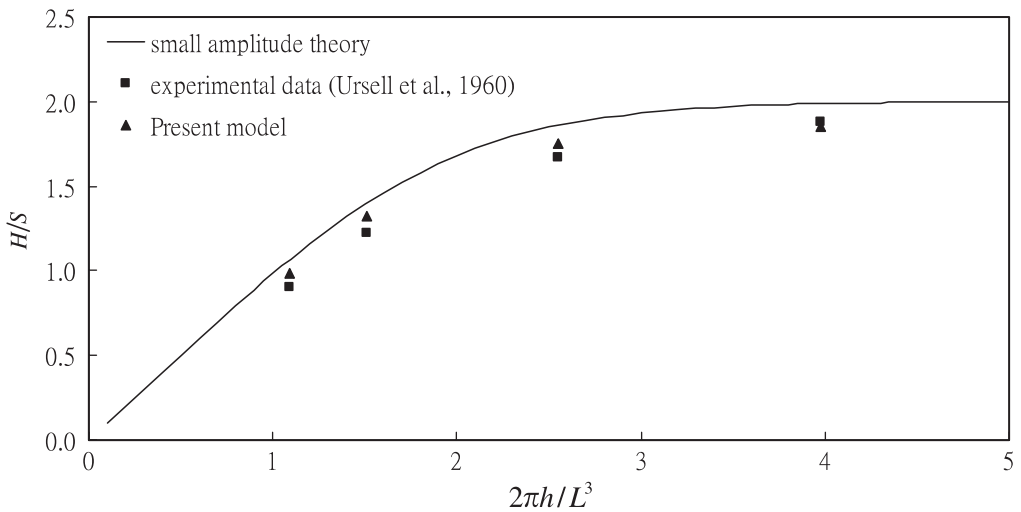

Figure 5. Comparison with the experimental data about the deviation from wavemaker theory due to finite wave steepness.

wave height in the range of $x = 1.0$–3.0 m in order to compare with experimental data and the small-amplitude wave theory. This distance is far enough to avoid taking the evanescent waves into account in these cases. The comparisons are illustrated in Figure 5. For the case of deep water wave ($h/L > 0.5$), the numerical result matches to the experimental data quite well. While for the other cases, the wave heights generated by present model are slightly higher than experimental data, but still much lower than predicted by the small-amplitude wave theory. This demonstrates that the wave heights by the small-amplitude wave theory are

in general overpredicted. The nonlinearity plays a vital role for the finite-amplitude waves as far as wave heights are concerned.

4.2. *Monochromatic waves passing over a submerged obstacle*

Luth *et al.* [28] carried out laboratory wave generation tests, including breaking and non-breaking waves, in a physical wave flume in order to analyse the evolution of the frequency spectrum for waves travelling over a submerged structure. The layout of the physical wave flume is shown in Figure 6. When the present numerical model was applied, the downstream boundary was set up at 40 m to ensure that the effects from the downstream boundary are minimized. The test case of wave height 2.0 cm and wave period 2.02 s is chosen since the nonlinearity is the most dominant among non-breaking wave test runs. This test case was also numerically simulated by Gobbi and Kirby [29] by using a fourth order fully nonlinear Boussinesq-type equation model (named as FN4 in this paper) and by Li and Fleming [30] with a 3-D model directly solving the Navier–Stokes equations (named as DNS in this paper). Numerical simulations of free surface displacement at $x = 5.2$, 12.5, 14.5 and 17.3 m were illustrated in the paper of Li and Fleming [30] while numerical results of free surface displacement at $x = 2.0, 4.0, 5.7, 10.5, 12.5, 13.5, 14.5, 15.7, 17.3, 19.0, 21.0$ and 23.0 m were obtained in the paper of Gobbi and Kirby [29]. The available experimental data of Luth *et al.* [28] were measured at $x = 2.0, 4.0, 5.7$ (actually at 5.2m but stated at 5.7m), 10.5, 12.5, 13.5, 14.5, 15.7, 17.3, 19.0, 21.0 and 23.0 m. We try to compare all the experimental data as well as those two numerical results as much as possible in order to test the feasibility of present meshless numerical model.

Since Luth *et al.* [28] generated waves by a hinge-type wavemaker, the boundary condition at the wave paddle is different from that in Equation (15). The horizontal velocity at the left boundary is no longer vertically uniform. Therefore, we have to modify Equation (15) by specifying the position of the wave paddle in the following form:

$$\xi(z,t) = \frac{S(z+h)}{2h} \sin \omega t \tag{16}$$

Horizontal spacing of adjacent boundary points along the free surface has been tested and 0.1 m is found to be sufficient, as shown in Figure 7, though 0.05 m was suggested by Li and Fleming [30]. There are 806 source points outside the computational domain. The time step taken is 0.025 s.

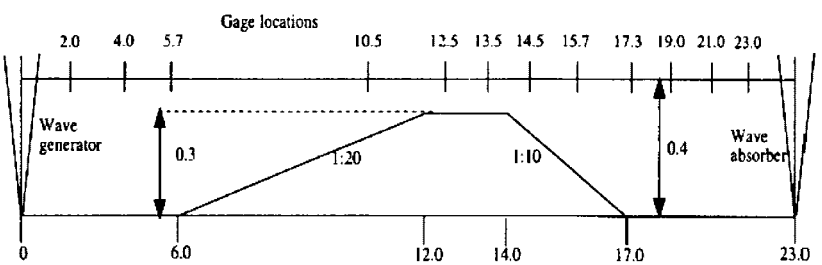

Figure 6. Sketch of wave flume of Delft experiments [28].

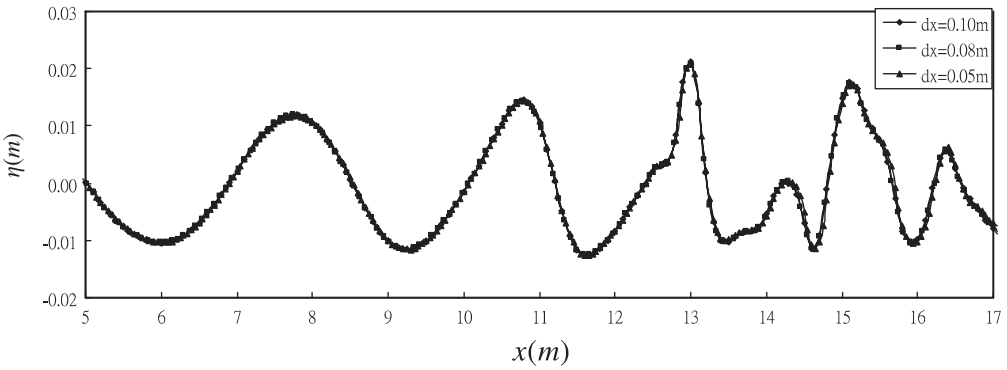

Figure 7. Results of different horizontal spacing of adjacent boundary points along the free surface.

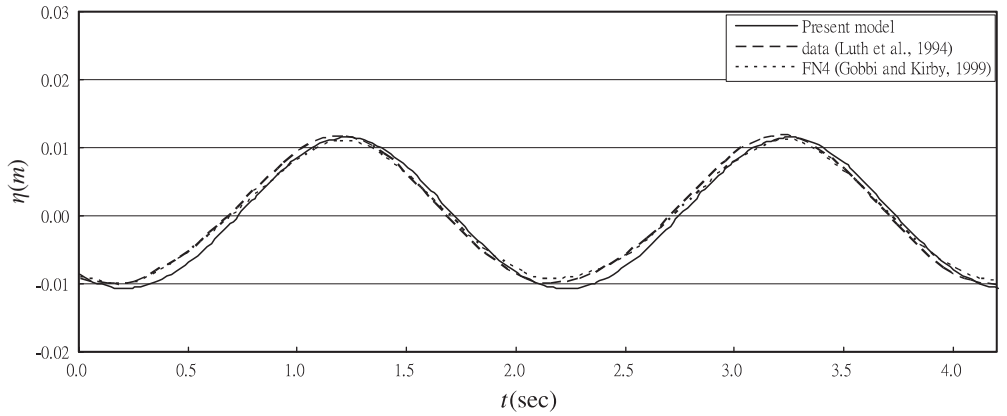

Figure 8. Comparison of computational free surface displacement with experimental data at $x = 2.0$ m.

Data for comparison were digitized from the paper of Gobbi and Kirby [29] and also the work of Li and Fleming [30]. The numerical results of free surface displacements for $x = 2.0, 4.0, 5.2, 5.7, 10.5, 12.5, 13.5, 14.5, 15.7, 17.3, 19.0$ and 21.0 m are illustrated in Figures 8–19, respectively. Figures 8 and 9 depict the comparisons of free surface displacements of experimental data with the present and Gobbi and Kirby [29] at $x = 2.0$ and 4.0 m, respectively. The three results are all very close to one another. The comparison of free surface displacements between the present solution with Li and Fleming [30] at $x = 5.2$ m is illustrated in Figure 10, in which one can observe that there is a little out of the phase between these two results. Numerical results of free surface displacement at $x = 5.7$ m for both the present and Gobbi and Kirby [29] also reveal some degree out of the phase as compared with experimental data, as shown in Figure 11. It was explained by Gobbi and Kirby [29] that the gage was actually located at $x = 5.2$ m while it was stated at $x = 5.7$ m in the provided information

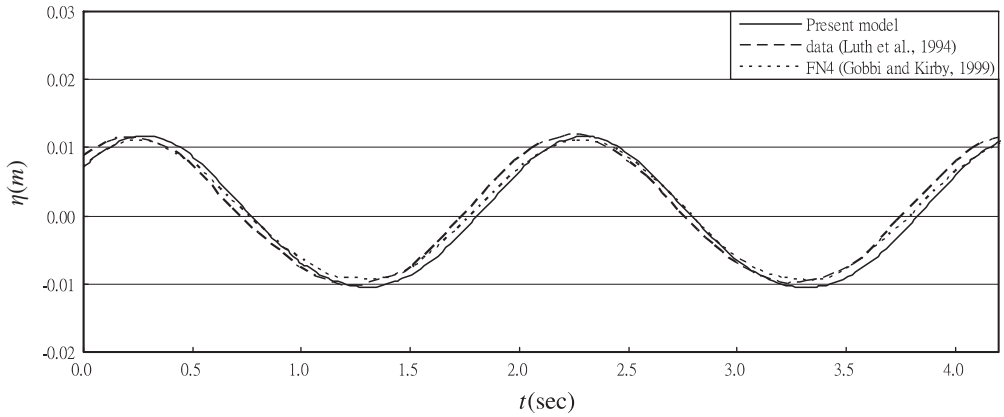

Figure 9. Comparison of computational free surface displacement with experimental data at $x = 4.0$ m.

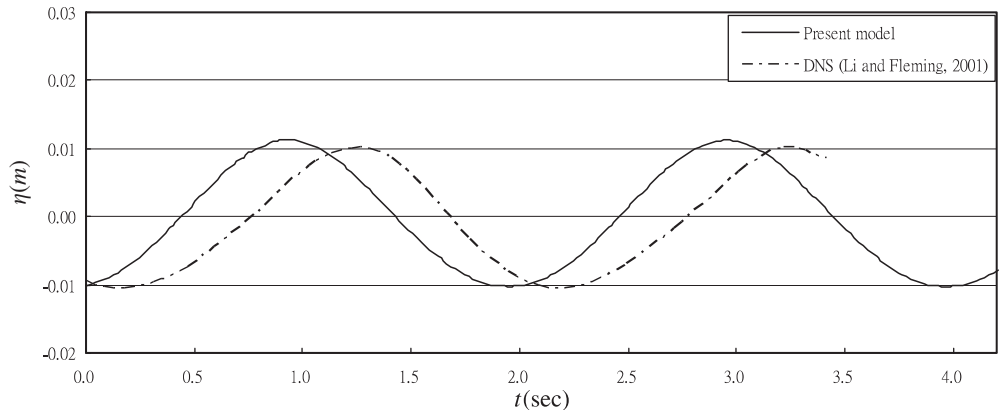

Figure 10. Comparison of computational free surface displacement with experimental data at $x = 5.2$ m.

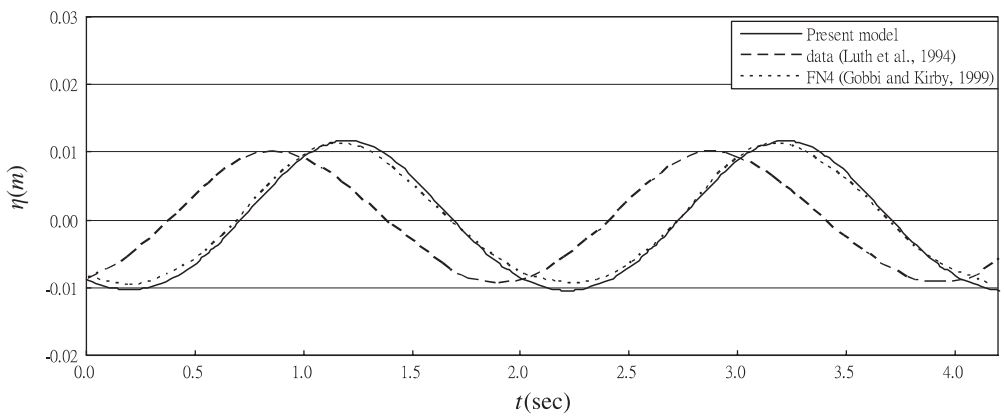

Figure 11. Comparison of computational free surface displacement with experimental data at $x = 5.7$ m.

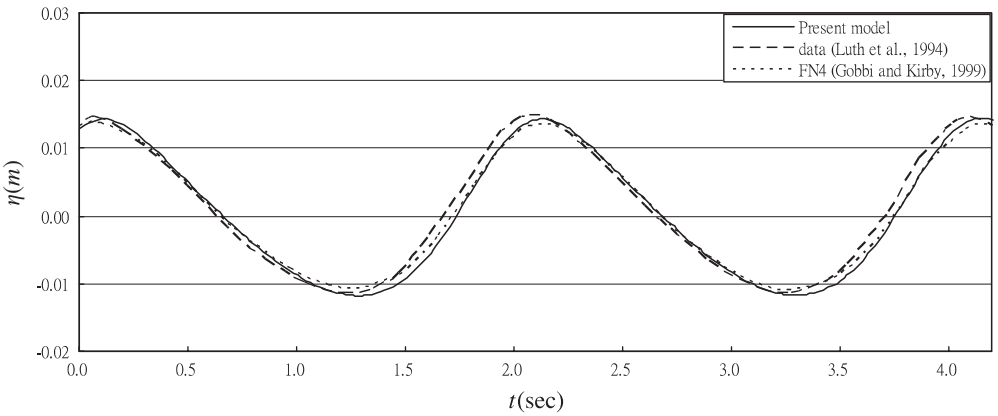

Figure 12. Comparison of computational free surface displacement with experimental data at $x = 10.5$ m.

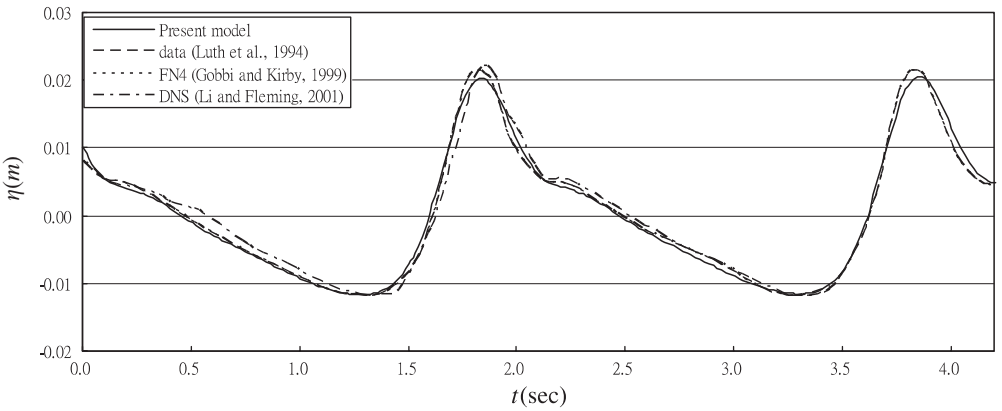

Figure 13. Comparison of computational free surface displacement with experimental data at $x = 12.5$ m.

of Luth *et al.* [28]. There was no mention if Li and Fleming [30] altered the position from $x = 5.7$ m to $x = 5.2$ m. We preferred not to alter the original information and leave this as a note at this moment. Numerical solutions at the gages upstream from the obstacle excellently match the physical model results except at $x = 5.7$ m, as depicted in Figures 8, 9 and 11. For the gages behind and over the obstacle, such as from $x = 10.5$, 12.5, 13.5, 14.5, 15.7, 17.3, 19.0 to 21.0 m, the comparisons of the numerical model solutions for the free surface displacements with the experimental data show that present model can be successfully used for nonlinear wave propagation and deformation, as well as the other two complex numerical models, as illustrating from Figures 12–19. However, much simpler efforts are reflected from the implementation of present meshless numerical approach.

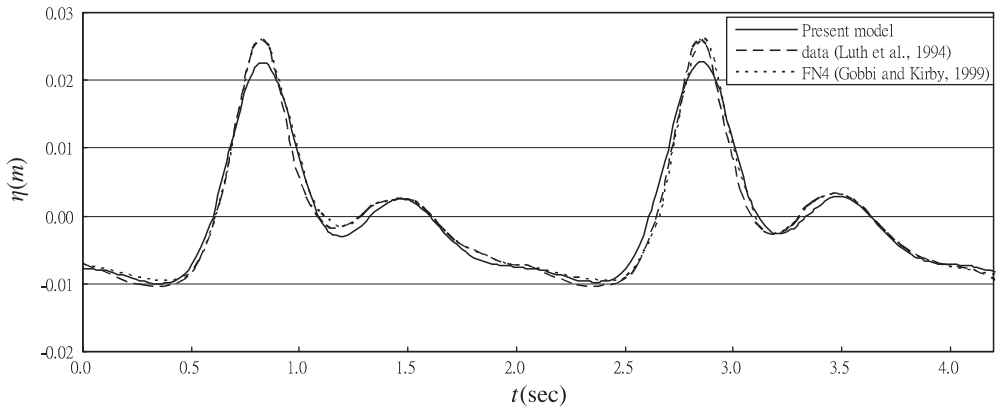

Figure 14. Comparison of computational free surface displacement with experimental data at $x = 13.5\,\mathrm{m}$.

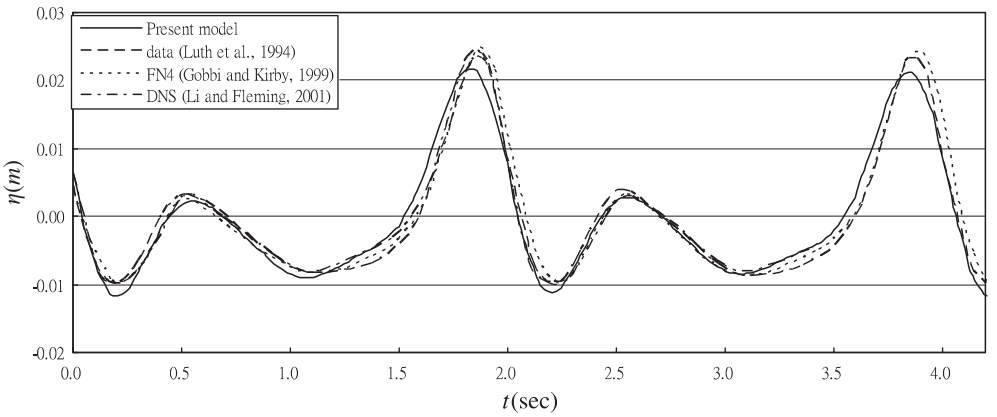

Figure 15. Comparison of computational free surface displacement with experimental data at $x = 14.5\,\mathrm{m}$.

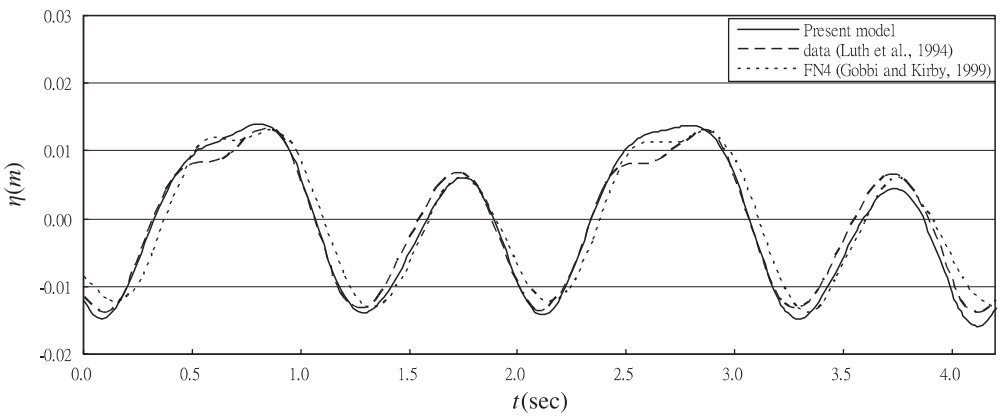

Figure 16. Comparison of computational free surface displacement with experimental data at $x = 15.7\,\mathrm{m}$.

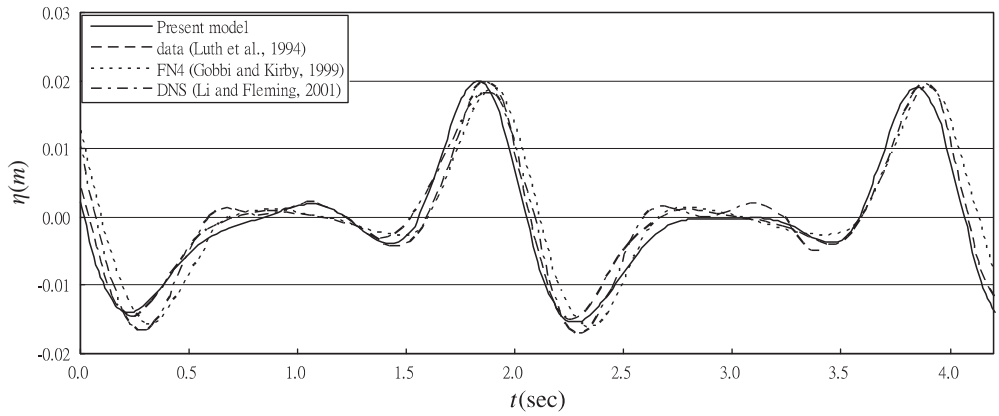

Figure 17. Comparison of computational free surface displacement with experimental data at $x = 17.3$ m.

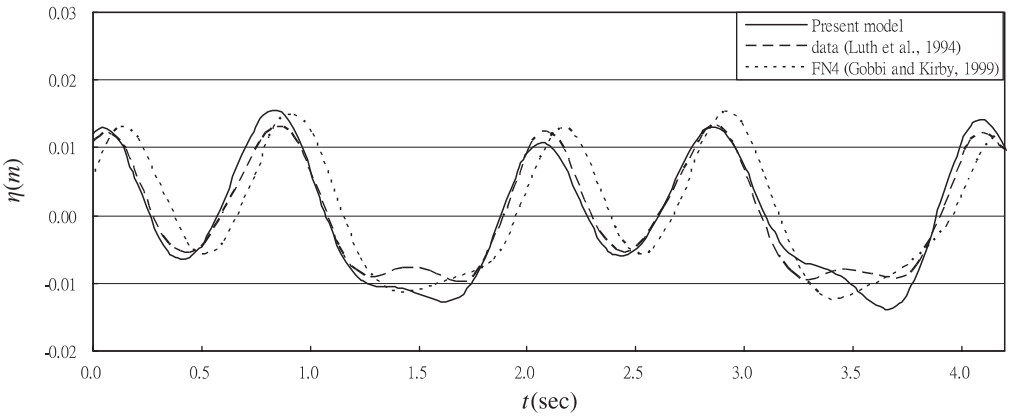

Figure 18. Comparison of computational free surface displacement with experimental data at $x = 19.0$ m.

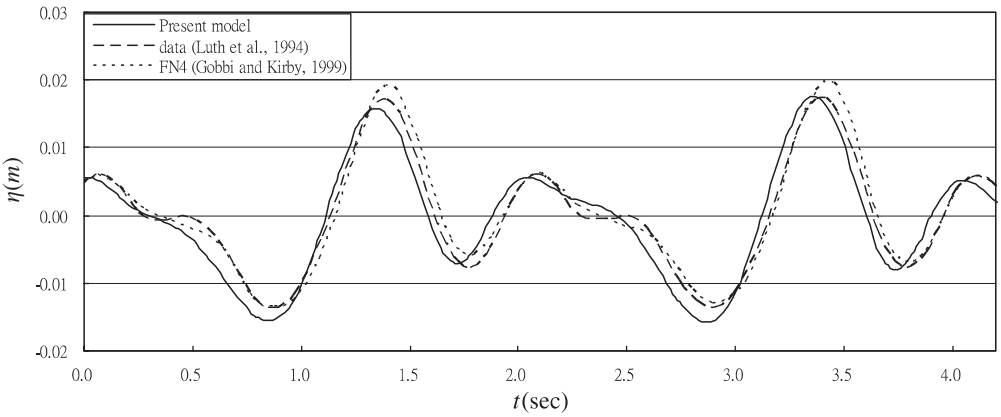

Figure 19. Comparison of computational free surface displacement with experimental data at $x = 21.0$ m.

5. CONCLUSIONS

This boundary-type meshless method requiring neither domain nor surface meshing is suitable for solving problems with deforming and/or moving boundaries. In free surface water wave problems, one can choose fundamental solution of the Laplace operator to be the form of the radial basis function so that only a few collocation points along the boundary are needed. The present numerical model, with neither prolix scheme formulation nor tediously iterating procedures, has provided an effective tool for simulating fully nonlinear free surface gravity water wave problems. In periodic wave generation simulation, this numerical wavemaker has successfully produced the periodic finite-amplitude waves with high wave-steepness, which characterizes the fully nonlinear water waves. We have compared the nonlinear wave propagation problem of monochromatic waves passing over a submerged obstacle through the formulations of direct numerical simulation of Navier–Stokes equations, the fourth order Boussinesq equation, and the Laplace equation. All the three models reveal different comparable modelling capabilities as compared with the experimental data. However, our model is the easier model among them to describe the salient features of the fully nonlinear water waves.

Though the present method also produces full and dense matrices which could take much time in solving the linear algebraic system, the computational speed is expected to accelerate once the effective matrices compressors, similar to the developments for BEM [18–20], were developed. Compared with the analogous BEM works [10–16], the present method with no need of singular surface integrations is easier to implement. Furthermore, the proposed approach for time marching is rather straightforward without any iterating procedures. Compared to the MEL approach, which needs numerical integration in time domain, computational time can be economized. However, since we treat the free surface displacement as a function of the horizontal plane, the overturning waves could not be simulated.

REFERENCES

1. Peregrine DH. Long waves on beach. *Journal of Fluid Mechanics* 1967; **27**:815–827.
2. Issacson M, Cheung KF. Second order wave diffraction around two-dimensional bodies by time domain method. *Applied Ocean Research* 1991; **13**:175–186.
3. Nwogu O. An alternative form of Boussinesq equations for near shore wave propagation. *Journal of Waterway, Port, Coastal, and Ocean Engineering* (ASCE) 1993; **119**:618–638.
4. Massel SR. Harmonic generation by waves propagating over a submerged step. *Coastal Engineering* 1983; **7**:357–380.
5. Vada T. A numerical solution of the second-order wave-diffraction problem for a submerged cylinder of arbitrary shape. *Journal of Fluid Mechanics* 1987; **174**:23–37.
6. Palm E. Nonlinear wave reflection from a submerged circular cylinder. *Journal of Fluid Mechanics* 1991; **233**:49–63.
7. Sulisz W. Diffraction of second-order surface waves by semisubmerged horizontal rectangular cylinder. *Journal of Waterway, Port, Coastal, and Ocean Engineering* (ASCE) 1993; **119**:160–171.
8. Glauss G. Dramas of the sea: episodic waves and their impact on offshore structures. *Applied Ocean Research* 2002; **24**:147–151.
9. Lo DC, Young DL. Arbitrary Lagrangian–Eulerian finite element analysis of free surface flow using a velocity–vorticity formulation. *Journal of Computational Physics* 2004; **195**:175–201.
10. Longuet-Higgins HS, Cokelet ED. The deformation of steep waves on water. I. A numerical method of computation. *Proceedings of the Royal Society of London* 1976; **A350**:1–26.
11. Issacson M. Nonlinear wave effects on fixed and floating bodies. *Journal of Fluid Mechanics* 1982; **120**: 267–281.
12. Dommermuth DG, Yue DKP. Numerical simulations of nonlinear axisymmetric flows with a free surface. *Journal of Fluid Mechanics* 1987; **178**:195–219.

13. Grilli ST, Skourup J, Svendsen IA. An efficient boundary element method for nonlinear water waves. *Engineering Analysis with Boundary Elements* 1989; **6**:97–107.
14. Cooker MJ, Peregrine DH, Skovggard O. The interaction between a solitary wave and a submerged semicircular cylinder. *Journal of Fluid Mechanics* 1990; **215**:1–22.
15. Ohyama T, Nadaoka K. Development of a numerical wave tank for analysis of nonlinear and irregular wave field. *Fluid Dynamics Research* 1991; **8**:231–251.
16. Grilli ST, Guyenne P, Dias F. A fully nonlinear model for three-dimensional overturning waves over an arbitrary bottom. *International Journal for Numerical Methods in Fluids* 2001; **35**:829–867.
17. Tsai WT, Yue DKP. Computation of nonlinear free-surface flows. *Annual Review of Fluid Mechanics* 1996; **28**:249–278.
18. Rokhlin V. Rapid solution of integral equations of classical potential theory. *Journal of Computational Physics* 1985; **60**:187–207.
19. Hackbusch W, Nowak ZP. On the fast matrix multiplication in the boundary element method by panel clustering. *Numerische Mathematik* 1989; **54**:463–491.
20. Beylkin G, Coifman R, Rokhlin V. Fast wavelet transforms and numerical algorithms I. *Communications on Pure and Applied Mathematics* 1991; **44**:141–183.
21. Hardy RL. Multiquadric equations of topography and other irregular surfaces. *Journal of Geophysical Research* 1971; **76**:1905–1915.
22. Franke C. Scattered data interpolation: test of some methods. *Mathematics of Computation* 1982; **38**:181–200.
23. Moody J, Darken C. Fast-learning in networks of local tuned processing units. *Neural Computation* 1989; **1**:281–294.
24. Kansa JE. Multiquadrics—a scattered data approximation scheme with applications to computational fluid dynamics—II. Solutions to parabolic, hyperbolic and elliptic partial differential equations. *Computers and Mathematics with Applications* 1990; **19**:127–145.
25. Wong SM, Hon YC, Golberg MA. Compactly supported radial basis functions for shallow water equations. *Applied Mathematics and Computation* 2002; **127**:79–101.
26. Golberg MA, Chen CS. *The Method of Fundamental Solutions for Potential*, *Helmholtz and Diffusion Problems*, *in Boundary Integral Methods—Numerical and Mathematical Aspects*. Computational Mechanics Publications: Southampton, Boston, 1998; 103–176.
27. Ursell F, Dean RG, Yu YS. Forced small amplitude water waves: a comparison of theory and experiment. *Journal of Fluid Mechanics* 1960; **7**:32–53.
28. Luth HR, Klopman G, Kitou N. Kinematics of waves breaking partially on an offshore bar; LDV measurements of waves with and without a net onshore current. *Technical Report H-1573*, Delft Hydraulics, Delft, The Netherlands, 1994.
29. Gobbi MF, Kirby JT. Wave evolution over submerged sills: tests of a high order Boussinesq model. *Coastal Engineering* 1999; **37**:57–96.
30. Li B, Fleming CA. Three-dimensional model of Navier–Stokes equations. *Journal of Waterway*, *Port*, *Coastal*, *and Ocean Engineering* (ASCE) 2001; **127**:16–25.

